Progress in Organic Coatings 163 (2022) 106657

Contents lists available at ScienceDirect

Progress in Organic Coatings

journal homepage: www.elsevier.com/locate/porgcoat

Effects of environmental conditions on the micro-mechanical properties of formulated waterborne coatings

J.L. Hall [a,c], A. Pérez [b], E.L. Kynaston [c], C. Lindsay [c], J.L. Keddie [a,*]

[a] Department of Physics, University of Surrey, Guildford, Surrey GU2 7XH, UK
[b] POLYMAT, University of the Basque Country UPV/EHU, Joxe Mari Korta Center, Avenida Tolosa 72, 20018 Donostia-San Sebastián, Spain
[c] Syngenta, Jealott's Hill International Research Centre, Bracknell, Berkshire RG42 6EY, UK

ARTICLE INFO

Keywords:
Latex
Hydroplasticization
Creep
Indentation
Relative humidity
Hardness

ABSTRACT

Waterborne colloidal polymer coatings are widely used in architectural and agricultural applications where they are subject to challenging environments, such as extremes of temperatures and relative humidities (RH). This research investigates the effects of adding two common co-formulants, poly(acrylic acid) (PAA) and xanthan gum (XG), to waterborne polymer composite coatings in these environments. The mechanical properties of the resulting coatings are of particular interest. Hardness, creep and tack properties of thick (~400 μm) formulated model coatings were characterized using a micro-indentation technique operating in a single cycle within a bespoke environmental chamber. Measurements were made at three temperatures (16, 20 and 30 °C), which span the glass transition temperature (T_g) of the acrylic copolymer binder, and over three RH values of 10%, 43%, and 90%. The creep data were analysed using the Burgers model to extract characteristic viscoelastic properties. The tack was found by recording the force when withdrawing the probe from the sample and using it to obtain nominal stress (knowing the indentation depth and probe geometry) during the indenter's withdrawal and hence the work of adhesion (W_{Adh}) to detach from the coating. Tack adhesion is completely lost below the binder's T_g but increases when the ambient temperature increases. In formulated coatings, both the tack and creep deformation increase as the relative humidity increases, and this trend is observed at each temperature. There is no evidence from thermal analysis for plasticization of the acrylic polymer by moisture sorption, but the two co-formulants are hydrophilic. The observed softening of the coatings at high RH can be attributed to water sorption in the components. The presence of glassy PAA has the effect of raising the hardness of glassy coatings, but only at low RH when there is no plasticization by water. The addition of hydrophilic XG surprisingly reduces tack adhesion while also raising the viscosity of the coating. These findings will inform the formulation of waterborne colloidal coatings to function in a range of environments.

1. Introduction

Colloidal polymers have myriad uses, such as in paints [1], adhesives [2], pharmaceuticals [3], and coatings for agricultural purposes [4–6]. Regardless of application, the mechanical properties of colloidal coatings usually define their performance in applications. To achieve the desired mechanical properties, proper film formation must occur. Latex film formation is a well-studied phenomenon characterized by solvent evaporation [7,8], particle coalescence [9,10], and interdiffusion of polymer chains across particle boundaries [11–13]. Film formation is often described by a sequence of stages, but in reality it is a continuous process, and its stages can overlap and influence each other. For instance, the final stage (interdiffusion) has been observed to occur even when water is still present in a coating, before particle deformation is complete [14].

Formulated waterborne coatings have numerous components, beyond the emulsion polymer that serves as a binder. Coatings for seeds are an illustrative example of such a formulated product, with the first formulations being developed in the 1930s for cereals [15]. Seed coatings are used to increase crop and vegetable yield, to aid ecological restoration [16,17,18], to change the physical properties of seeds (allowing easier handling), and to deliver active ingredients [15,19]. In addition to the binder, which can be a synthetic colloidal polymer, formulations typically include inorganic fillers (to increase weight, size,

* Corresponding author.
E-mail address: j.keddie@surrey.ac.uk (J.L. Keddie).

https://doi.org/10.1016/j.porgcoat.2021.106657
Received 2 August 2021; Received in revised form 26 November 2021; Accepted 29 November 2021
Available online 15 December 2021

and reduce cost), rheology modifiers, dispersants for fillers and other additives, nutrients, soil adjuvants, and pigments or tracers [6]. Some of these ingredients impart hydrophilicity, such as the polymers used to disperse filler particles and soil adjuvants [20].

After film formation, formulated coatings used in foods, pharmaceuticals, agriculture, and outdoor infrastructure are exposed to liquid water or extremes of humidities, across a range of temperatures, when they are in use. The typical multi-component formulation of coatings adds another level of complexity when characterizing and explaining the effects of environmental conditions on properties. Therefore, an important consideration when formulating coatings is the possibility of plasticization of polymers by adsorbed water, known as hydroplasticization, not only during film formation but also when the final product is in use. Hydroplasticization can occur even with trace quantities of bound water [21].

The focus of previous research on hydroplasticization has primarily been on the reduction of the glass transition temperature (T_g) and the bulk properties, such as the dynamic modulus, with increased water sorption [22–24]. However, one might also expect the surface properties - such as the hardness, wetting, friction, and tack adhesion - to be affected to a greater extent than the bulk, in cases where water is being adsorbed from the atmosphere at the air interface. There has been comparatively little exploration of how the surface mechanical properties of coatings are affected by environmental factors, especially relative humidity (RH). Chen et al. [25] speculated that a high RH could affect the surface mechanical properties of coatings, but did not provide direct measurements. However, in their intriguing research, indentations in nominally glassy polymer surfaces were observed to flow out and flatten when under a high RH [25]. They attributed their observation to the effects of hydroplasticization, even though their acrylic polymer was not hygroscopic. Other studies found that a high RH correlated with adhesion loss at a coatings interface with a substrate [26] and increased crack propagation in adhesive joints [27], but these effects are not associated with hydroplasticization.

Hydroplasticization is especially prevalent in applications where coatings are subject to high levels of liquid water, such as in coatings for medication [28–30]. Coatings formulations become increasingly sensitive to hydroplasticization when hydrophilic additives, such as salts and dispersants, are added [31]. In numerous industries, xanthan gum, which is a polysaccharide [32], is used as a rheology modifier. Xanthan gum is known to adsorb and bind large quantities of water from the vapor [33] due to its hydrophilicity. This bound water could potentially affect the mechanical properties of a final coating and hence is of interest in this present research.

The bulk mechanical properties of polymers are often studied by axisymmetric large-strain analysis and by dynamic mechanical analysis (DMA) [34]. DMA has also been used to study the properties of formulated colloidal composite coatings [35], such as those containing silica [36], titania [37], and $CaCO_3$ [38,39]. Usually free-standing materials (that is, materials not bound to a substrate) are studied by DMA and large-strain analysis. Test specimens are typically 1 mm or more in thickness, rather than having a thickness on the order of tens of micrometers, which is more typical for protective coatings.

A powerful technique for the mechanical characterization of samples in the form of coatings on a substrate is indentation. The Oliver-Pharr method of measuring hardness and elastic modulus via indentation was first introduced in 1992 [40] and refined in 2004 [41]. It is widely used to characterize mechanical behavior of materials on nano- and micro-scales. One of its most appealing qualities is its ability to provide mechanical properties directly from indentation load-displacement curves, without the need to image the indenter's impression and measure its area. This technique can also be used to characterize plastic deformation and the time-dependent properties of viscoelastic materials, e.g. creep under a fixed load. Although initially developed for the Berkovich indenter, the method applies to a variety of axisymmetric indenter geometries, such as spherical [24] and conical indenters [42].

In this work, we have developed a single characterization cycle using an indenter to evaluate the hardness, elasticity, and viscoelasticity of the near-surface region. Additionally, we measure the energy dissipated when withdrawing the indenter from the coating, as an indication of the tack adhesion. We indent into the surface over distances of micrometers, which is well below the thickness of the coating.

One advantage of micro-indentation (rather than nano-scale deformation) is the comparable length scales of the indenter and the features within a formulated coating (i.e. $CaCO_3$ protruding at the sample surface, ranging from a few hundred nanometers to a few micrometers). Mapping surfaces with large surface features (above a few micrometers) using atomic force microscopy (AFM) is often impossible. Indenting composite materials using a nano-indenter has the potential to characterize the mechanical properties of the binder and the filler separately but not to characterize the properties of the entire composite. We use micro-indentation as a tool to investigate length scales between that of DMA (bulk properties) and nano-indentation (nano-scale properties of the individual components) with most of the information being obtained from the surface.

In this research, we consider a model formulated coating in which two key additives, xanthan gum and PAA, are added to a synthetic colloidal acrylic copolymer binder at various ratios. Here, xanthan gum is used to represent a rheology modifier in the formulation, and PAA represents a typical waterborne dispersant. We investigate the resulting coating in both the rubbery and glassy regimes through variation of the experimental temperature. We control the RH during sample storage and during the experimental procedure, to assess the extent to which these hydrophilic xanthan gum and PAA additives affect the mechanical properties of the near-surface region, as measured via our micro-indentation technique. We assess the effects of temperature, RH, and composition on the elastic, viscoelastic and adhesive properties of the formulated coatings. Our experimental technique provides an intermediate between the characterization of bulk materials via DMA or large-strain tensile deformation and the analysis of purely surface phenomena via techniques such as atomic force microscopy (AFM) and nano-indentation.

2. Materials and methods

2.1. Latex synthesis

A seed latex was prepared by emulsion polymerization of styrene (St), butyl acrylate (BA) and acrylic acid (AA). A solution of sodium dodecyl sulfate (SDS, 18 g) and sodium hydrogen carbonate (1.3 g) in de-ionized water (740 g) was prepared. The solution was bubbled with nitrogen for 20 min at 70 °C and stirred at 200 RPM. Potassium persulfate initiator (1.3 g) in de-ionized water (10 g) was added and a solution of St/BA/AA (450 g, 49:49:1 by weight) was added over 3 h. The reaction was held at 70 °C for another hour and then heated to 90 °C overnight to fully decompose remaining initiator. The product was a latex with 37% solids content with particle size 40 nm and >99% monomer conversion as measured by gravimetry. This latex was then used in a seeded semi-batch emulsion polymerization process.

The seed latex (175 g), sodium hydrogen carbonate (0.75 g), potassium persulfate initiator (0.75 g) and water (300 g) were mixed together. The mixture was purged with nitrogen for 20 min and heated to 70 °C. A solution of St/BA/AA (606 g, 49:49:1 by weight) was added over 3 h. Following complete monomer addition the reaction was held at 70 °C for 1.5 h before being cooled to room temperature. This procedure is adapted from [43] The particle size of the seed and the final latex was found using dynamic light scattering (Malvern Zetasizer Nano Series, Malvern, UK). The product was a latex with 40% solids content with particle size 89 nm and > 98% monomer conversion as measured by gravimetry. Hereafter, the copolymer in the latex dispersion will be called P(St-BA-AA).

2.2. Coating formulation

The latex was diluted to 30 wt% using de-ionized water for use in formulation. This blank formulation is referred to hereafter simply as Latex. Table 1 lists the compositions of each formulation along with the names used to describe each. A 2 wt% solution of xanthan gum (XG) (Rhodopol 23, Solvay) in water was prepared. The aqueous solutions of xanthan gum contained 0.4 wt% dipropylene glycol solution of 1,2-benzisothiazolin-3-one (Proxel GXL, Lonza) as a biocide to prevent spoilage from bacteria, yeasts, and fungi. For simplicity, xanthan gum (as a model rheology modifier) and the biocide are jointly referred to hereafter as XG. The formulation with a small amount (0.2 wt%) of added XG is called Latex (XG). Poly(acrylic acid) (PAA) was used as a model dispersant in some formulations. A PAA solution (sodium salt, average M_w~8000 g/mol, 45 wt% in H_2O, Sigma Aldrich) was added to formulations to achieve a final concentration of either 0.3 wt% (called PAA Low) or 1.0 wt% (called PAA High). Finally, both XG and PAA (at two different concentrations) were included in formulations, referred to as PAA Low (XG) and PAA High (XG). After adding one or more co-formulants to the original latex dispersion, the formations were mixed for at least 16 h on a roller.

2.3. Film formation

The formulated mixtures described in Section 2.2 and Table 1 were spread onto clean glass substrates (76 mm × 52 mm). The coatings were placed in an oven in air held at 30 °C for 24 h to ensure complete film formation. The resulting coatings had a thickness of approximately 400 m. The thicknesses were measured using digital calipers and recorded prior to mechanical testing. Following film formation, the coatings were placed in one of three bespoke chambers (Fig. S1 in the Supplementary materials) with humidity-controlled environments (RH values of 10%, 43%, or 90%). The three different RH environments were created using open containers of silica gel, saturated K_2SO_4 solution, and de-ionized water, respectively. The coatings were left at room temperature in the humidity-controlled chambers to reach equilibrium, typically for one week. The final compositions of the dry coatings are shown in Table 2.

2.4. Micro-indentation

Analysis of the hardness, viscoelasticity, and tack adhesion of the coatings was carried out using a single cycle on a micro-indenter (Texture Analyser, Stable Micro Systems, Godalming, Surrey). A conical, stainless-steel indenter with its semi-angle at the apex of $\alpha = 70.3°$ (as in [42]) was used to indent the samples. The indenter tip was polished to minimize its surface roughness and cleaned manually using fibre-free tissue paper and acetone between measurements. The contact area of the indenter, A, is related to the depth of indentation, h, through the angle, α, as $A = \pi h^2 tan^2\alpha = 24.5h^2$.

Prior to measurements, coatings were stored in environmental chambers that were designed to enable fast and easy attachment to the micro-indenter. Thus, the samples were both stored and analysed inside the humidity chambers with minimal disruption. The chambers were also designed to allow lateral movement, so samples were probed in multiple locations along one plane without disruption to the RH and temperature inside the chamber. Two Peltier modules (TEC1-12706), fitted with heat sinks and 12 V fans attached to either side of the module, were used inside the chambers to control the temperature. Three temperatures (16 °C, 21 °C, and 30 °C) were chosen to investigate how the mechanical and tack adhesion properties change across the sample T_g. The temperature and relative humidity were monitored using three Arduino-controlled sensors (Telaire T9602 IP67 Harsh Environment Humidity & Temperature Sensor, ±2% RH, ±0.5 °C). See the configuration in Fig. S1 (Supplementary materials). The samples were allowed to reach the set temperature for 1 h before micro-indentation experiments began.

Table 1
Sample nomenclature and percentage weight of each component for wet formulated mixtures.

	Composition (wt%)			
Sample name	P(St-BA-AA)	PAA	XG	H_2O
Latex	30.0	0.0	0.0	70.0
Latex (XG)	30.0	0.0	0.2	69.8
PAA Low	27.9	0.3	0.0	71.8
PAA High	23.1	1.0	0.0	75.9
PAA Low (XG)	27.9	0.3	0.2	71.6
PAA High (XG)	23.1	1.0	0.2	75.7

Table 2
Sample nomenclature and percentage weight of each component for dried coatings.

	Composition (wt%)		
Sample name	P(St-BA-AA)	PAA	XG
Latex	100.0	0	0
Latex (XG)	99.3	0	0.7
PAA Low	98.8	1.2	0
PAA High	95.7	4.3	0
PAA Low (XG)	98.1	1.2	0.7
PAA High (XG)	94.8	4.3	0.9

An example of the micro-indentation cycle in the experiments is given in Fig. 1. This figure presents an example of the entire force-distance cycle (a), with the extraction of the raw creep data (distance-time) (b), and the raw tack adhesion data (force-distance) (c). For each coating, a minimum of three indentations were made in different positions. The values of properties repeated hereafter are the mean of at least three replicates.

At the start of a testing cycle, the conical probe was brought into contact with the coating surface at a speed of 0.1 mm/s. A maximum load of 0.98 N was applied for 300 s. At this load the relative indentation depth was typically 40% or less, which is well within the allowed limit of over 50% deformation for a soft coating on a hard substrate [44]. The indenter was then moved away from the coating at a speed of 0.1 mm/s. The force and vertical position of the indenter (i.e, related to the indentation depth, h) were recorded over time throughout the cycle. The contact area, A, was calculated from h. The coating's hardness, H, was calculated by dividing the load of 0.98 N by A at the point in time when the maximum load was first reached. To study the creep in the coating under the constant load, the nominal strain, ε, over time during the hold, was determined by dividing h by the initial thickness, h_0. Thus, ε was recorded as a function of time. During the creep experiment, the conical indenter pushes deeper into the coating over time, t, thus increasing A, and reducing the nominally applied stress σ, which is defined as the load divided by A. As is shown in Fig. 1, during the unloading, a negative value of force was sometimes recorded when there was adhesion between the indenter and the coating. The position at which the force reached zero when unloading was taken to define the position of zero strain in a tack adhesion curve.

2.5. Burgers model analysis

The viscoelasticity observed during the creep experiment was analysed using the Burgers model. According to this model, [34] the time-dependent strain, $\varepsilon(t)$, for a constant applied stress, σ, is given by the sum of contributions from the elastic, viscous, and viscoelastic responses acting in series:

$$\varepsilon\left(t\right) = \frac{\sigma}{E_H} + \frac{\sigma}{\eta_N}t + \frac{\sigma}{E_K}\left(1 - exp\left[-\frac{E_K}{\eta_K}t\right]\right) \quad (1)$$

The value of σ used in our creep analysis corresponded to the

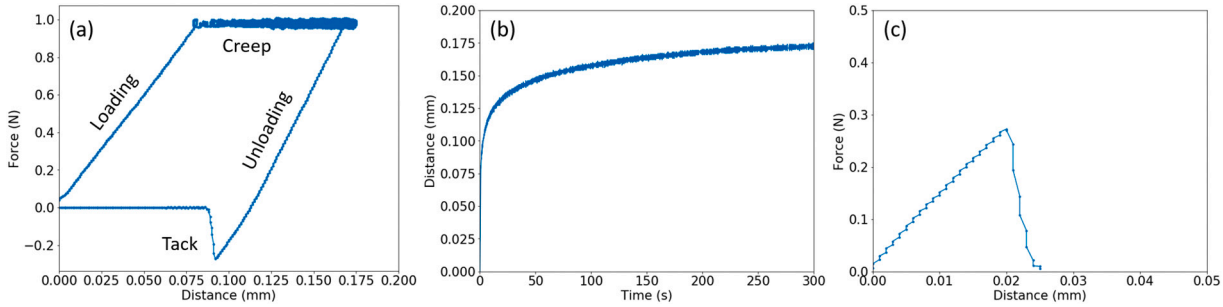

Fig. 1. (a) An example of the recorded data in an indentation cycle on a Latex (XG) coating when indented at 20 °C and 43% RH. (b) shows the raw creep profile for the same sample and test conditions, and (c) shows the raw tack adhesion profile for that same experiment.

maximum indentation depth at the end of the 300-s hold. The elastic response (first term on the right) is characterized by the Hookean modulus, E_H. The viscous response (change over time, t, in the second term on the right) is characterized by the Newtonian viscosity, η_N. Finally, the viscoelastic response is characterized by the Kelvin modulus and viscosity, E_K and η_K, respectively. η_K/E_K defines a characteristic relaxation time, τ. The Burgers model is typically applied to bulk specimens under a tensile or compressive stress. In this analysis, we applied the model under a constant indentation load. During the creep of the indenter, the stress decreased as the area increased, and this change is ignored here. The numerical values of the extracted parameters depend on the definition of the particular definition of the strain in the coating. Our intention in this analysis is to be able to compare the properties under various environmental conditions rather than to obtain absolute values.

A Python script was used to fit the Burgers model to the recorded $\varepsilon(t)$ data with a fixed value of σ. The script uses a non-linear least squares method while varying four parameters: E_H, η_N, E_K, and η_K, iterating 500,000 times to improve the fit, minimizing the residuals between the model and the data. Specifically, we used the scipy.optimize package with the curve_fit function, using the Levenberg-Marquardt algorithm to vary and optimize the parameters. Mean values of the viscoelastic parameters are extracted, using the standard error to find uncertainty.

2.6. Tack adhesion analysis

At temperatures above their T_g, some of the coatings had measurable tackiness. Hence, the same analysis that is used for the probe-tack tests on pressure-sensitive adhesives was applied [45], although typically probe-tack experiments use a spherical or flat-punch probe and a short contact time of a few seconds. When withdrawing the indenter from the coatings, there was often an opposing force caused by the tack adhesion. The force to withdraw the indenter was measured as a function of distance above the coating. The nominal stress, σ, was found from the measured load divided by A at the start of unloading. The energy of adhesion upon the probe withdrawal (W_{Adh}) of a coating with an initial thickness h_0 was calculated as [46]:

$$W_{Adh} = h_0 \int_0^{\varepsilon_{max}} \sigma\left(\varepsilon\right) d\varepsilon \tag{2}$$

where $\varepsilon_{\max}$ is the maximum strain reached at the point of detachment of the probe from the coating surface. Eq. (2) was used to find W_{Adh} of each sample, when there was a measurable force. As the thicknesses of the coatings were very similar in value, comparison of W_{Adh} values between samples is valid. Values of work obtained by integration of the force-distance curves were close in value to those of W_{Adh}. The latter analysis is used here because it will allow easier comparison to values in the literature for PSAs.

2.7. Microscopy

2.7.1. Scanning electron microscopy

A scanning electron microscope (JEOL JSM-7100F) was used to obtain images of sample surfaces. Samples were stored in desiccators for one week to remove moisture before sputter coating with 6 nm of Au to prevent charging during imaging. Images were obtained using an accelerating voltage of 5 kV and a probe current of 6 nA. Energy-dispersive X-ray (EDX) spectroscopy analysis was used to obtain elemental maps. A higher probe current of 10 nA and an accelerating voltage of 10 kV was used for EDX analysis to increase the number of counts.

2.7.2. Atomic force microscopy

The mixtures described in Section 2.1 and Table 1 were spread onto clean cover glasses (18 mm×18 mm). The coated cover glasses were placed in an oven in air held at 30 °C for 24 h to ensure complete film formation. The samples were stored in humidity-controlled chambers held at 10%, 43%, and 90% relative humidity for a minimum of one week to allow equilibration then analysed using an atomic force microscope (Dimension Edge, Bruker) and NanoScope Analysis software. Note that the relative humidity was not controlled during the AFM experiment.

Scans used triangular silicon cantilevers (ScanAsyst Air, Bruker) equipped with an ultrasharp, conical silicon tip, with a tip radius of 2 nm. The nominal resonant frequency f_0 of the cantilever was about 70 kHz and its spring constant k was about 0.4 N/m. Images were recorded in the topographic (height) mode and in the adhesion mode.

2.8. Thermal analysis

A differential scanning calorimeter (DSC Q1000, TA Instruments) was used to carry out thermal analysis on samples containing varying amounts of water. Samples of xanthan gum and PAA were independently dried in an oven at 30 °C for 24 h before being stored in humidity-controlled chambers held at 10%, 43%, and 90% relative humidity for a minimum of one week to allow equilibration. Approximately 10 mg of each sample was placed in an aluminium hermetic pan, calibrated in nitrogen.

A heat-cool-heat cycle was used in all measurements. For samples stored under the lower RH, the temperature was equilibrated at −50 °C before heating to 120 °C at a rate of 10 °C/min. The temperature was then reduced to −50 °C at a cooling rate of 10 °C/min before heating back to 120 °C at a rate of 10 C/min to complete the cycle. For samples stored under the highest humidity, the initial temperature was reduced to −100 °C°C to ensure the T_g of the hydroplasticized material was visible.

Thermogravimetric analysis was performed on solution-cast XG material after storage of at RH of 10% or 90%. Measurements were made on samples (7–8 mg) in a nitrogen atmosphere using a TGA Q500 instrument from TA Instruments (New Castle, USA). The temperature was

ramped from room temperature at 10 °C/min.

3. Results and discussion

Before the presentation of the mechanical properties under the various environmental conditions, we first consider water interaction with the components.

The sorptive capacity of the monomers in the copolymer must be considered to explain possible hydroplasticization. The equilibrium sorption of water from the vapor phase by the latex binder and the co-formulants is expected to be described by an isotherm in which sorption increases with water activity and RH. According to data in the literature, at an RH of 50%, the water sorption of the CH_2 groups in the butyl acrylate is negligible, but its acrylic group (−(C=O)-O-) will sorb 0.05 mol at the same RH [47]. One mole of the styrene rings will absorb only 0.002 mol of water, making this monomer the most hydrophobic of the three. In contrast, protonated carboxylic acid groups in AA are the greatest sorbants of water, with 0.3 mol sorbed per mole of COOH at an RH of 50% [47]. However, in the copolymer, the AA is present at a low concentration of only 1% by weight. Despite the high sorptive capacity of AA, it is in too low a concentration to greatly reduce the copolymer's T_g as measured by DSC after storage at 90% RH. This result can be seen in Table 3, where there are negligible differences between the T_g of the P (St-BA-AA) copolymer after storage at 10% RH and 90% RH. The values obtained from the first and second heatings are comparable in value. There is an increase in the T_g on the order of 2 °C, which can be attributed to the loss of trace amounts of plasticizing water during the first heating, but the effect is small.

The copolymer itself is not plasticized significantly by the presence of sorbed water, but one of the added components, PAA, certainly is (Table 3). Here, there is a clear and obvious decrease in the T_g when the PAA is stored under a higher RH. Poly(acrylic acid) is a well-studied polymer, and its dry T_g has previously found to be 103 °C [48]. The concentration of added PAA is comparable to the AA in the copolymer, however the added PAA is a sodium salt solution. The sodium counterion leads to additional water sorption, beyond that of PAA and AA in the copolymer. This explains the differences between the water sorption of PAA (as an added component) and the St-BA-AA copolymer. Fig. S2 (Supplementary materials) shows the DSC thermogram for PAA stored at 10% RH, presenting a fairly broad T_g with a main transition at approximately 39 °C. It is possible that some water within the sample at 10% storage RH and/or the effect of the sodium salt present in the original solution has contributed to this broad T_g, which is much lower than that found in previous work. No transitions indicating melting or freezing are observed, which means that free water is not present.

When analyzing XG in the same way, it was difficult to identify a T_g at all. However, previous work has shown that the T_g of powdered XG can vary between −16.4 and −23.3 °C in a water activity range of 0.11 to 0.84 [49]. Note that there are differences in the samples we have measured, namely that our XG solution also contains a biocide to prevent spoiling; and the DSC sample was not analysed in powdered form but when cast from solution. Our thermogravimetric analysis confirmed that the XG sorbs water from the vapor. When XG was stored at an RH of 10%, there was a 5.8% mass loss at temperatures up to 100 °C from water loss. However, when the RH of storage has at 90%, the mass loss of water when heating to 100 °C in TGA rose to 16.4 wt%. This difference in mass loss is attributed to additional water sorbed at the higher RH. There was additional bound water that was not liberated until temperatures rose above 100 °C.

DSC experiments performed on the formulated coatings showed little effect of the storage RH on the measured T_g. See Table S1 in the Supplementary materials. There was often no visible thermal transition that could be attributed to the additive (PAA and/or XG) in the DSC thermogram, despite it being possible to see clear transitions in the data for pure PAA. This lack of extra transition is likely because of the small amounts in which the co-formulants were added (only up to 4.3% PAA in the dry coating, and up to 0.9% XG in the dry coating), which is beneath the sensitivity of the technique. There are no phase transitions that would suggest the presence of free water.

Having established that the thermal properties are not strongly affected by the RH, we next consider the mechanical properties. Example creep indentation curves are shown shown in Fig. 2 for Latex (XG) coatings stored at three different RH. Time zero is set as the time when the maximum load of 0.98 N is reached. In each curve, there is a fast elastic response leading to a sharp increase in the strain. Over the longest times, there is a straight-line and positive increase in strain, which arises from viscous flow. At intermediate times, the curvature is caused by a combined viscous and elastic response. It can be seen in the figure that data are described very well by the Burgers model (superimposed as the solid black line). Notably, the relative humidity has a strong and noticeable effect on the shapes of the creep curves. There is a greater strain for the coating stored at an RH of 90% and a steeper slope at the longer times. Quantitative analysis of the creep data will be presented later in Section 2.3. First, however, hardness and adhesion will be discussed.

3.1. Hardness and Hookean modulus

The hardness of the indented coatings was found using the method described in Section 2.4. The hardness as a function of both temperature and RH for the Latex coating is shown in Fig. 3(a). There is a noticeable drop in the hardness when the analysis temperature (30 °C) is above the T_g of the Latex sample. This obvious result is explained by a softening of the coating when in the rubbery state. There is no obvious correlation between the RH and hardness. As described in Section 3 there is only 1 wt% AA in the copolymer, and the styrene and butyl acrylate monomers have relatively small sorptive capacities, resulting in little-to-no hydroplasticization under a higher RH.

Table 3
Glass transition temperatures for each constituent ingredient stored at three different relative humidities. Results from the first and (second) heating are shown.

	T_g (°C)		
	Relative humidity		
Sample	10%	43%	90%
P(St-BA-AA)	24.6 (23.2)	- (-)	23.0 (25.4)
PAA	39.0 ([a])	9.7 (9.4)	−44.8 ([a])

[a] Indicates that a value could not be obtained from the DSC thermograms.

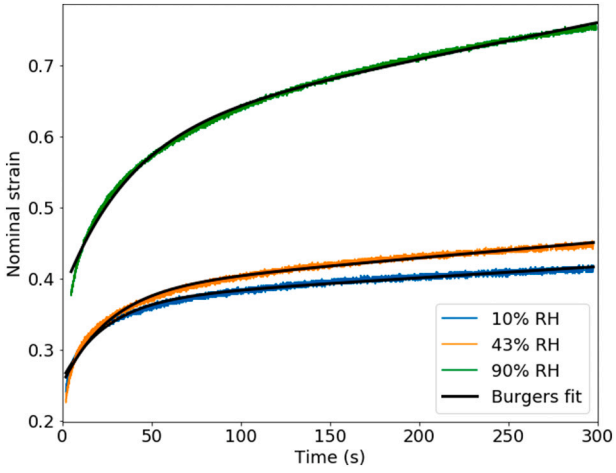

Fig. 2. Three creep data sets and corresponding fits to the Burgers model for Latex (XG) coatings indented at 20 °C at three different RH: 10%, 43%, and 90%.

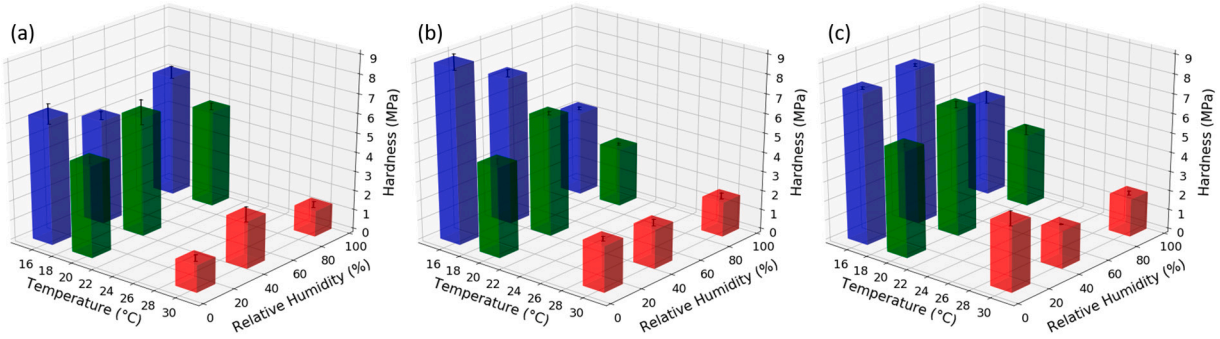

Fig. 3. Average hardness under a range of environmental conditions (RH and temperature) for the storage of three types of coating: (a) Latex, (b) Latex (XG), and (c) PAA Low.

The average hardness for Latex (XG) is shown in Fig. 3(b). As the RH increases, the hardness decreases, particularly at low temperatures. This result can be explained by the presence of the hydrophilic xanthan gum, with its already low , softening as the RH increases. As noted already, however, the effects of water sorption were not observed in the thermal analysis.

With an increased temperature, the hardness also decreases. At 30 °C, there ceases to be a strong humidity effect as high temperatures become the dominant reason for the lowering of the hardness. A similar correlation between hardness and increasing RH is seen for the PAA Low sample (Fig. 3 (c)) which suggests that the added PAA is being softened in the presence of high RH. This observation is despite the DSC thermograms showing no effect of the RH, which provides a note of warning upon over-reliance solely on thermal analysis.

Hardness data for the other three samples (PAA High, PAA Low (XG), and PAA High (XG)) are shown in Fig. S7 (Supplementary materials). These three samples each exhibit softening both when the temperature increases and when the RH increases, although at high temperatures the RH-dependence becomes weaker as the effects of the increased temperature dominate.

The effects of additives in the formulation are most apparent at the lowest temperature (16 °C) where the latex binder is glassy. When the RH is lowest, the addition of a small amount of XG (0.7 wt%) in Latex XG or a small amount of PAA (1.2 wt%) in PAA Low raises the hardness to 8.5 MPa and 7.5 MPa, respectively. There could be a reinforcement of the composite arising from the presence of the additives around the colloidal particles. However, when the RH is raised to 90% at the lowest temperature, there is a pronounced effect on the hardness. The values for the Latex (XG) and the PAA Low fall below the value for Latex, most likely because of the hydroplasticization of the additives.

Analysis of the creep indentation data provides values of the Hookean elastic modulus. Its calculation is similar to the determination of the hardness from the indentation. Hence, as would be expected, the trends in E_H are the same as found for the hardness. The results are presented in Fig. S8 (Supplementary materials). Most notable is the decrease in E_H at 16 °C for the Latex XG sample from 14.8 MPa at low RH to 3.2 MPa at high RH, which is a drop of 71.4%.

3.2. Work of adhesion

Next, the debonding of the indenter from the coating surface is considered. As an example, Fig. 4 shows how the measured tack adhesion of PAA Low increases with RH. In these tack curves, the sharp drop in the stress at a particular strain signals the debonding. When the RH is at the highest value of 90%, both the maximum stress and the strain when debonding are much higher than at the two lower RH. Together, these effects lead to a higher W_{Adh} at the highest RH. Furthermore, the gradient of the initial linear region in the stress-strain curve is lower at the higher RH, which means that the elastic modulus is lower, which is consistent with the prior analysis. The greater extension before debonding can be explained by a greater dissipative component in the viscoelasticity in the presence of higher RH.

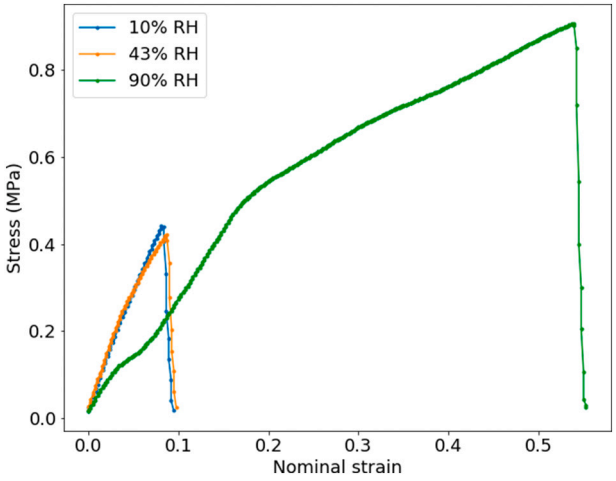

Fig. 4. Three representative tack curves for PAA Low after being indented at 20 °C at three different RH: 10%, 43%, and 90%.

Fig. 5 (a) shows the combined effects of temperature and RH on the W_{Adh} for Latex samples. Increasing the temperature to above the T_g clearly increases the adhesion to the probe, whereas increasing the RH leads to a decreased W_{Adh} at 30 °C. The largest W_{Adh} value of 650 Jm^{-2} is found at the lowest RH. This is a surprising effect for two reasons. Firstly, there are no added hydrophilic components, so a trend between W_{Adh} and RH was not expected. Secondly, this effect is the opposite to what would be expected with any hydrophilic component, as with an increased RH, the hydrophilic polymers should soften and hence W_{Adh} should increase. Indeed, it has been reported previously that tack increased when the storage modulus decreased below a threshold value as the temperature was raised [50].

Previous research on pressure-sensitive adhesives has shown that the work of adhesion is influenced by surface energy (and hence the composition of a surface), wetting (requiring a sufficiently low viscosity), and the resistance to deformation during debonding (i.e. the dissipative component of the viscoelasticity) [45]. One explanation for the Latex result is that free water, present at interparticle boundaries and voids, could reduce adhesion as the indenter geometry essentially comes into contact with pockets of liquid water. The water component cannot support stress during debonding. We observed that the Latex films noticeably whitened when stored under high humidity, because of the effect of light scattering from the water pockets [51], supporting this hypothesis. An additional experiment was performed to investigate the effects of water pockets.

After film formation, a Latex coating was heated for an additional 24

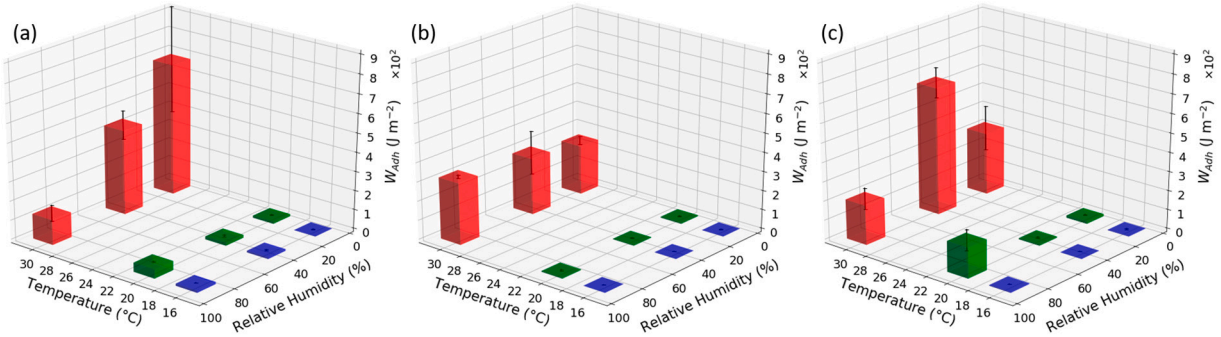

Fig. 5. Average work of adhesion for (a) Latex, (b) Latex (XG), and (c) PAA Low held and tested in various environmental conditions. Note that the axes are reversed in comparison to the other figure, as a way to increase visibility.

h in the oven at 60 °C to drive additional particle coalescence. It was then stored at 90% RH for one week before following the micro-indentation procedure described in Section 2.4. The annealed sample showed a much higher work of adhesion (660 ± 34 Jm^{-2}) than a reference Latex coating without the annealing step (130 ± 21 Jm^{-2}) because of a greater maximum stress and greater strain when debonding, see Fig. S9 (Supplementary materials). The water whitening effect was much less pronounced for the Latex sample after heating compared to the original state. The visual difference, plus the tack adhesion result, support the concept that with the elimination of water pockets along with greater cohesion from additional coalescence, the tack adhesion increases.

To gain more insight into the adhesion of the Latex surface, AFM analysis was performed. The surface structure, in combination with adhesion at the nano-scale, was investigated. Adhesion maps, along with topographical images, for Latex coatings that had been stored at the three different humidities before imaging at room temperature are presented in 6. Light patches in the adhesion maps, which correspond to areas of higher adhesion, are attributed to “islands” of surfactant enrichment at the sample surface, because Latex samples contain no additives. The coverage of the surfactant islands was greater for the Latex stored at the two higher RH. (Note, however, since the overall image area is small using AFM, there's a high chance to either “miss” these islands completely, or to “hit” an island that masks most of the underlying latex particles (as in (b)). Conclusions were drawn from multiple observations.) In the sample at 10% RH, small circular spots of surfactant cover only a small fraction of the surface area. The increase in surfactant coverage with increasing RH is consistent with previous research [52], where the effect was attributed to greater surfactant mobility with greater surfactant hydration.

It is also insightful to compare the AFM adhesion maps with the tack adhesion at the macro-scale. As the RH increased, the magnitude of difference in the adhesion force between the surfactant islands and surrounding, nominally clean, polymer binder increased. This enhanced adhesion could stem from surfactant molecule mobility being enhanced by water sorption. At the bulk scale at 20 °C, Fig. 5 (a)), the measured adhesion is relatively low for each RH, but with increased RH there is a slight increase in adhesion.

To present the effects of formulation with XG, Fig. 5 (b) shows W_{Adh} over the range of conditions. The W_{Adh} remains relatively constant over the range of RH at each temperature, and at 20 °C and 16 °C the value W_{Adh} is negligible at every RH. The lack of a strong effect of RH could be due to the already low T_g of XG, which is already in the rubbery regime at every temperature, meaning that it is a soft component under all conditions. Indeed the hardness of Latex (XG) showed only a weak dependence on RH, with the effect most obvious at the lowest temperature.

As was also found for the Latex coating, W_{Adh} is higher at 30 °C for Latex (XG), which can understood from the softening of the binder. However, the addition of a soft XG component does not translate here to greater deformation during debonding. Surprisingly, there is no evidence for tackiness being imparted by the addition of XG, despite it being viscoelastic. One explanation is that XG is not enriched at the coating surface where it could contribute directly to adhesion to the indenter.

Formulation with PAA is considered next. At 20 °C and 90% RH there is a relatively high W_{Adh} value (Fig. 5 (c)) when compared to both Latex and Latex (XG) under the same conditions. This result is consistent with softening of the PAA present at the sample surface. At 30° there is not a simple trend between RH and W_{Adh}, with the highest adhesion seen at the intermediate RH of 43%. This is possibly related to the heterogeneity of the surface, and this possibility was investigated using SEM analysis. Fig. 7 shows an SEM image of the surface of PAA Low alongside the corresponding EDX analysis of the same area. There is an island-like structure on the PAA Low surface, and the islands are enriched in Na which can largely be attributed to the sodium ions present in the original PAA solution. This image suggests that despite only 1.2 wt% PAA in the formulated coating, there is a relatively high abundance at the sample surface, which suggests an exudation of the PAA to the surface during film formation. Fig. 8 shows the same analysis for PAA High, where a denser coverage of PAA islands is inferred. Other examples of SEM images of these sample surfaces over larger areas can be seen in Figs. S11-S13. Fig. S13 shows clear phase separation, which could influence the measured tack adhesion depending on the particular region of indentation. If tested on nano-scale areas the variability is expected to be much stronger.

Fig. 6 shows adhesion maps for Latex which had been stored at a range of humidities before imaging at room temperature. There are no additives, so light patches which correspond to areas of higher adhesion can be attributed to surfactant (SDS) rising to the sample surface. The measured adhesion is relatively low for each sample (also evident for Latex samples indented at 20 °C, Fig. 5 (a)), but with increased humidity there is a slight increase in adhesion.

For completeness, W_{Adh} data for (a) PAA High, (b) PAA Low (XG), (c) and PAA High (XG) are shown in the the Supplementary materials, Fig. S10. In each of these samples the most important factor in determining the level of tack adhesion is the temperature. The experiments performed at 30 °C show the highest W_{Adh} for every sample because the polymer is softened above its T_g, and there is only a slight increase in W_{Adh} when the RH increases. A simple yet important conclusion is that the formulation, including the combination of XG and PAA, suppresses the tack adhesion of the coating surfaces.

3.3. Newtonian viscosity

The Newtonian viscosity, η_N, was extracted from the creep data by fitting to the Burgers model, as was described in Section 2.5. The viscous region corresponds to the linear part of the curve at the end of the stress-strain plot shown in Fig. 2.

Fig. 9 (a) shows the Newtonian viscosity of Latex under the various

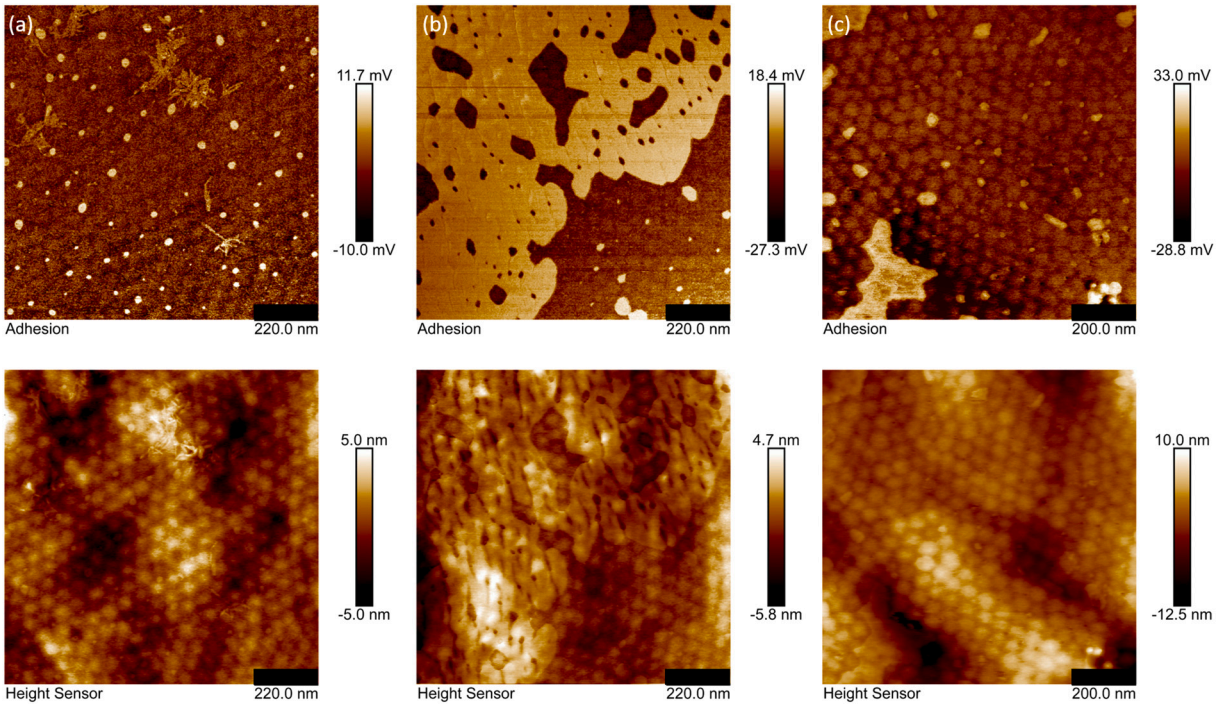

Fig. 6. Adhesion maps (top) and height maps (bottom) of Latex stored at (a) 10% RH, (b) 43% RH, (c) and 90% RH for a period of one week. All samples stored and imaged at room temperature.

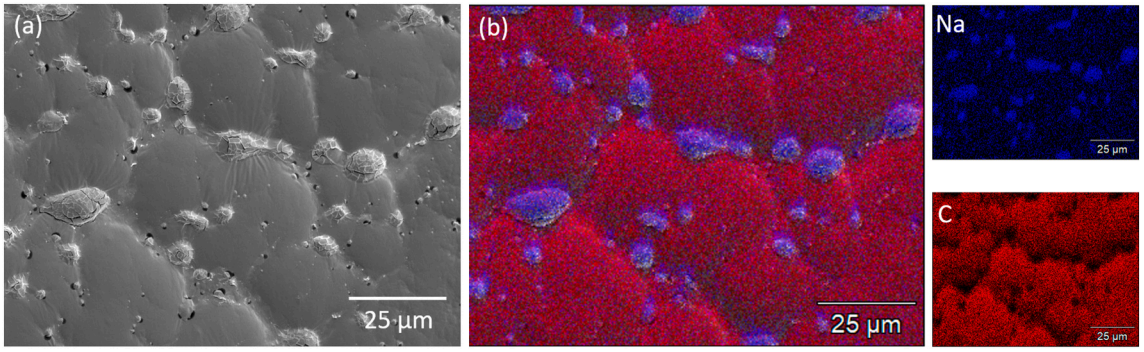

Fig. 7. (a) SEM image with (b) EDX analysis of the surface of PAA Low, stored at 10% RH for a period of one week, highlighting the presence of C and Na. Areas rich in sodium correspond to the PAA sodium salt solution.

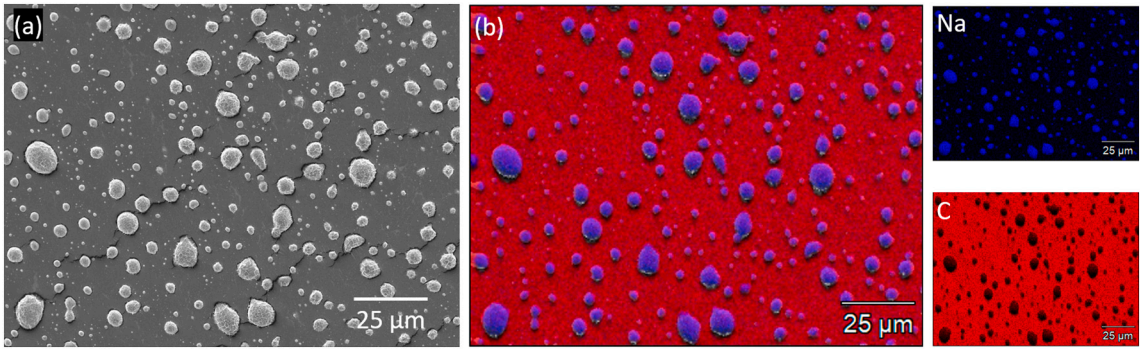

Fig. 8. (a) SEM image with (b) EDX analysis of the surface of PAA High, stored at 10% RH for a period of one week, highlighting the presence of C and Na. Areas rich in sodium correspond to the PAA sodium salt solution.

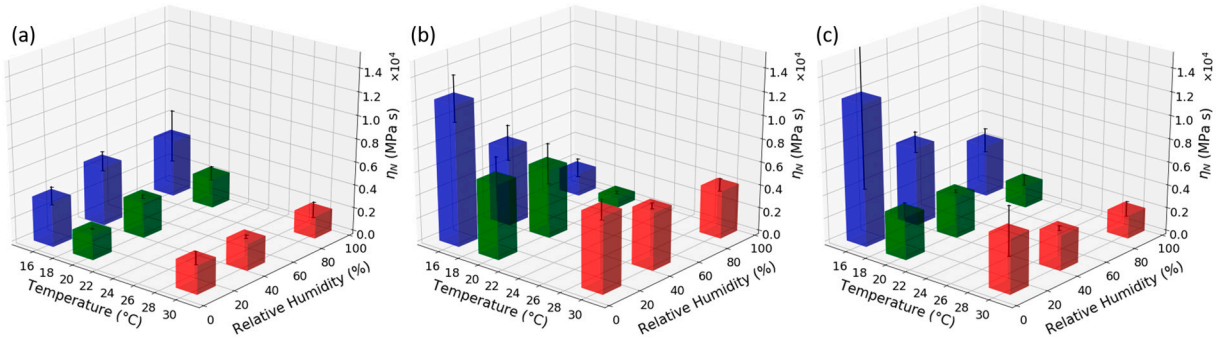

Fig. 9. Average Newtonian viscosity of (a) Latex, (b) Latex (XG), and (c) PAA Low held in various environmental conditions.

environmental conditions. Increasing the temperature decreases the viscosity, which is expected from the exponential dependence on the inverse of temperature temperature, such as is given by an Arrhenius relation [53]. In these experiments, with only three temperatures, fitting to this equation would not be meaningful. In general, there is no effect of changing RH on the viscosity for Latex samples.

The effect of the XG co-formulant is found by comparison to Fig. 9(b). The addition of XG increased the viscosity under all but two environmental conditions, when compared to Latex (Fig. 9 (a)). The two exceptional conditions for which the Latex XG's η_N is lower than for Latex are 90% RH at 16 °C and at 20 °C. The presence of plasticized XG at the boundaries between glassy particles might be enabling some additional flow, which is not possible for the glassy particles on their own. The addition of XG also increases the sensitivity to RH, as there is a marked decrease in η_N as RH increases, particularly at lower temperatures, closer to the T_g of XG as reported by Basu et al. [49]. This result demonstrates that the particular state of the XG present at low concentrations has a marked influence on the flowability.

Fig. 9 (c) shows the average viscosity for PAA Low. Generally speaking, there is a decrease in viscosity as the RH increases. The viscosity values are comparable to Latex (XG), but are lower than Latex (XG) at almost every environmental condition. There is also an expected decrease in η_N as the temperature is increased.

To complete the creep analysis, the relaxation time, τ, is presented for all samples over the range of conditions in Fig. S14 (Supplementary materials). This parameter depends strongly and inversely on temperature, which is expected for the exponential dependence of τ on temperature as given by the well-known Williams-Landel-Ferry equation [53]. There is also a slight reduction in τ as RH increases at 16 °C for samples when a co-formulant is added.

More results on η_N are provided in Fig. S15 (Supplementary materials), where PAA High, PAA Low (XG), and PAA High (XG) are considered. For all three samples there is an apparent reduction in η_N with increased RH and temperature, with the highest viscosity typically occurring at the lowest temperature and RH (16 °C, 10% RH), when the co-formulants are expected to be most solid-like.

4. Conclusions

We have used a micro-indentation technique in a bespoke environmental chamber to probe simultaneously the mechanical and adhesive properties of the near-surface region of viscoelastic polymer coatings. We have investigated how relative humidity and temperature influence the hardness, viscoelasticity, and tack adhesion of formulated coatings. We examined how additives in the formulation (a model thickener and a dispersant, individually and in combination) influence these properties over a range of environmental conditions.

PAA, a common dispersant, becomes hydroplasticized by water vapor at high RH, displaying a measurable reduction in T_g according to DSC analysis. A common rheology modifier, xanthan gum, does not display clear T_g s in DSC thermograms, regardless of storage RH, but absorbs measurable amounts of water from the vapor phase. However, the T_g of powdered XG is known to vary between −16.4 and -23.3 °C in a water activity range of 0.11 to 0.84 [49], and was not expected to impart a hardening to the formulation.

Despite no significant changes in the T_g of formulated coatings with varying RH, there is a clear change in their viscoelasticity, confirmed by fitting the Burgers model to creep data obtained using micro-indentation. There are also significant differences in the tack adhesion of coatings when exposed to high RH environments. In a general trend, adding PAA or XG causes the sample to become sensitive to RH.

When PAA is used as a co-formulant, at the highest RH, the hardness and viscosity are usually lower than in Latex, whereas the tack adhesion increases. Increasing the temperature above the T_g of P(St-BA-AA) binder has the same effect, and often overrides any trend with RH as it becomes the dominating factor. These results underscore the necessity for mechanical characterization to determine effects of hydroplasticization rather than relying solely on thermal analysis.

The addition of XG also has some surprising effects. At the lowest RH, when it is not expected to be plasticized, the addition of XG to Latex raises the hardness, whereas it softens the coating at high RH. Likewise, XG raises the viscous component of the coatings, most strongly at low RH. Furthermore, XG suppresses the tack adhesion at temperatures above the binder's T_g, possibly because it is not enriched at the coating surface and has a hardening effect on the bulk material.

Our results show that formulations and environmental conditions must be considered in combination, and that thermal analysis alone is not sufficient when attempting to understand coating performance in challenging environments. Our use of micro-indentation, rather than nano-indentation or bulk DMA, provides a simple, yet powerful, way to study a range of surface and viscoelastic properties on an intermediate length scale. These results could be used by formulators in the future to develop coatings for targeted applications.

CRediT authorship contribution statement

J.L. Hall: Conceptualization, Formal analysis, Investigation, Methodology, Visualization, Writing – original draft. **A. Pérez:** Methodology, Resources. **E.L. Kynaston:** Resources, Supervision, Writing – review & editing. **C. Lindsay:** Conceptualization, Resources, Supervision, Writing – review & editing. **J.L. Keddie:** Conceptualization, Methodology, Supervision, Writing – review & editing.

Declaration of competing interest

The authors declare that they have no known competing financial interests or personal relationships that could have appeared to influence the work reported in this paper.

Acknowledgements

This work was funded by EPSRC (Grant EP/L016788/1) through the Doctoral Training Centre in Micro- and NanoMaterials and Technology (MiNMaT). We benefited from useful discussions with Dr. Marco Ramaioli (INRAE, AgroParisTech - Center de Massy) and Dr. Nicholas Ballard (University of the Basque Country). We thank Violeta Doukova and Dave Jones (University of Surrey) for laboratory assistance and Dr. Agata Gajewicz-Jaromin for performing DSC and TGA analyses. We also thank Dr. James Adams (Cubica Technology) for his assistance in writing data analysis scripts. We thank Richard Turner (Acal BFI UK Ltd.) for the relative humidity and temperature probes, and for his assistance with their setup.

Appendix A. Supplementary data

Supplementary data to this article can be found online at https://doi.org/10.1016/j.porgcoat.2021.106657.

References

[1] Hanne M. van der Kooij, Joris Sprakel, Watching paint dry; more exciting than it seems, Soft Matter 11 (32) (2015) 6353–6359.
[2] Amel Bellamine, Elise Degrandi, Matthias Gerst, Rüdiger Stark, Cornelis Beyers, Costantino Creton, Design of nanostructured waterborne adhesives with improved shear resistance, Macromol. Mater. Eng. 296 (1) (2011) 31–41.
[3] Florence Lecomte, Juergen Siepmann, Mathias Walther, Ross J. MacRae, Roland Bodmeier, Polymer blends used for the coating of multiparticulates: comparison of aqueous and organic coating techniques, Pharm. Res. 21 (5) (2004) 882–890.
[4] Patrick Mulqueen, Recent advances in agrochemical formulation, Adv. Colloid Interf. Sci. 106 (1–3) (2003) 83–107.
[5] Alfred Elbert, Matthias Haas, Bernd Springer, Wolfgang Thielert, Ralf Nauen, Applied aspects of neonicotinoid uses in crop protection, Pest Manag. Sci. 64 (11) (2008) 1099–1105.
[6] Simone Pedrini, David J. Merritt, Jason Stevens, Kingsley Dixon, Seed coating: science or marketing spin? Trends Plant Sci. 22 (2) (2017) 106–116.
[7] Marcel Visschers, Jozua Laven, Rob van der Linde, Forces operative during film formation from latex dispersions, Prog. Org. Coat. 31 (4) (1997) 311–323.
[8] Alexander F. Routh, Drying of thin colloidal films, Rep. Prog. Phys. 76 (4) (2013), 046603.
[9] J.W. Vanderhoff, E.B. Bradford, W.K. Carrington, The transport of water through latex films, in: Journal of Polymer Science: Polymer Symposia volume 41, Wiley Online Library, 1973, pp. 155–174.
[10] Marcel Visschers, Jozua Laven, Anton L. German, Current understanding of the deformation of latex particles during film formation, Prog. Org. Coat. 30 (1–2) (1997) 39–49.
[11] Önder Pekcan, Ertan Arda, Void closure and interdiffusion in latex film formation by photon transmission and fluorescence methods, Colloids Surf. A Physicochem. Eng. Asp. 153 (1–3) (1999) 537–549.
[12] Yongcai Wang, Mitchell A. Winnik, Polymer diffusion across interfaces in latex films, J. Phys. Chem. 97 (11) (1993) 2507–2515.
[13] T.P. Russell, V.R. Deline, W.D. Dozier, G.P. Felcher, G. Agrawal, R.P. Wool, J. W. Mays, Direct observation of reptation at polymer interfaces, Nature 365 (6443) (1993) 235–237.
[14] Katja Pohl, Jörg Adams, Diethelm Johannsmann, Correlation between particle deformation kinetics and polymer interdiffusion kinetics in drying latex films, Langmuir 29 (36) (2013) 11317–11321.
[15] Glen Kaufman, Seed coating: a tool for stand establishment; a stimulus to seed quality, HortTechnology 1 (1) (1991) 98–102.
[16] Matthew D. Madsen, Kirk W. Davies, C. Jason Williams, Tony J. Svejcar, Agglomerating seeds to enhance native seedling emergence and growth, J. Appl. Ecol. 49 (2) (2012) 431–438.
[17] Matthew D. Madsen, Kirk W. Davies, Daniel L. Mummey, Tony J. Svejcar, Improving restoration of exotic annual grass-invaded rangelands through activated carbon seed enhancement technologies, Rangel. Ecol. Manag. 67 (1) (2014) 61–67.
[18] Mary I. Williams, R. Kasten Dumroese, Deborah S. Page-Dumroese, Stuart P. Hardegree, Can biochar be used as a seed coating to improve native plant germination and growth in arid conditions? J. Arid Environ. 125 (2016) 8–15.
[19] Suemar Alexandre Gonçalves Avelar, Fabianne Valéria de Sousa, Guilherme Fiss, Leopoldo Baudet, Silmar Teichert Peske, The use of film coating on the performance of treated corn seed, Rev. Bras. Sementes 34 (2) (2012) 186–192.
[20] Masoume Amirkhani, Hilary S. Mayton, Anil N. Netravali, Alan G. Taylor, A seed coating delivery system for bio-based biostimulants to enhance plant growth, Sustainability 11 (19) (2019) 5304.
[21] John G. Tsavalas, Donald C. Sundberg, Hydroplasticization of polymers: model predictions and application to emulsion polymers, Langmuir 26 (10) (2010) 6960–6966.
[22] Benjamin Voogt, Hendrik P. Huinink, Sebastiaan J.F. Erich, Jurgen Scheerder, Paul Venema, Joseph L. Keddie, Olaf C.G. Adan, Film formation of high t g latex using hydroplasticization: explanations from nmr relaxometry, Langmuir 35 (38) (2019) 12418–12427.
[23] Benjamin Voogt, Henk Huinink, Loes van de Kamp-Peeters, Bart Erich, Jurgen Scheerder, Paul Venema, Olaf Adan, Hydroplasticization of latex films with varying methacrylic acid content, Polymer 166 (2019) 206–214.
[24] Zhangwei Chen, Xin Wang, Alan Atkinson, Nigel Brandon, Spherical indentation of porous ceramics: elasticity and hardness, J. Eur. Ceram. Soc. 36 (6) (2016) 1435–1445.
[25] Qi Chen, Mingwen Tian, Kristel de Vos, Maud Kastelijn, Ron A.H. Peters, Joachim Loos, Jurgen Scheerder, Recovery dynamics of acrylic coating surfaces under elevated relative humidity monitored by atomic force microscopy, Prog. Org. Coat. 146 (2020), 105712.
[26] Kar Tean Tan, Bryan D. Vogt, Christopher C. White, Kristen L. Steffens, Joshua Goldman, Sushil K. Satija, Cyril Clerici, Donald L. Hunston, On the origins of sudden adhesion loss at a critical relative humidity: examination of bulk and interfacial contributions, Langmuir 24 (17) (2008) 9189–9193.
[27] A.J. Kinloch, C.F. Korenberg, K.T. Tan, J.F. Watts, Crack growth in structural adhesive joints in aqueous environments, J. Mater. Sci. 42 (15) (2007) 6353–6370.
[28] O. Bley, J. Siepmann, R. Bodmeier, Characterization of moisture-protective polymer coatings using differential scanning calorimetry and dynamic vapor sorption, J. Pharm. Sci. 98 (2) (2009) 651–664.
[29] Rong-Kun Chang, Krishnaswamy S. Raghavan, Munir A. Hussain, A study on gelatin capsule brittleness: moisture tranfer between the capsule shell and its content, J. Pharm. Sci. 87 (5) (1998) 556–558.
[30] Ewart T. Cole, Dominique Cadé, Hassan Benameur, Challenges and opportunities in the encapsulation of liquid and semi-solid formulations into capsules for oral administration, Adv. Drug Deliv. Rev. 60 (6) (2008) 747–756.
[31] Elena Jubete, Christopher M. Liauw, Norman S. Allen, Water uptake and tensile properties of carboxylated styrene butadiene rubber based water born paints: models for water uptake prediction, Prog. Org. Coat. 59 (2) (2007) 126–133.
[32] E.R. Morris, Polysaccharide rheology and in-mouth perception, in: Food Polysaccharides and Their Applications, Am Stephen, 1995.
[33] Paltu Banerjee, Indrajyoti Mukherjee, Subhash Bhattacharya, Sidhhartha Datta, Satya P. Moulik, Diptabhas Sarkar, Sorption of water vapor, hydration, and viscosity of carboxymethylhydroxypropyl guar, diutan, and xanthan gums, and their molecular association with and without salts (nacl, cacl2, hcook, ch3coona, (nh4) 2so4 and mgso4) in aqueous solution, Langmuir 25 (19) (2009) 11647–11656.
[34] Haochuan Wang, Darla Graff Thompson, Jon R. Schoonover, Steven R. Aubuchon, Richard A. Palmer, Dma- ftir creep- recovery study of a poly (ester urethane) elastomer with molecular-level viscoelastic modeling, Macromolecules 34 (20) (2001) 7084–7090.
[35] Dan Y. Perera, Effect of pigmentation on organic coating characteristics, Prog. Org. Coat. 50 (4) (2004) 247–262.
[36] Emmanuelle Chabert, Michel Bornert, Elodie Bourgeat-Lami, J.-Y. Cavaillé, Remy Dendievel, Catherine Gauthier, Jean-Luc Putaux, André Zaoui, Filler–filler interactions and viscoelastic behavior of polymer nanocomposites, Mater. Sci. Eng. A 381 (1-2) (2004) 320–330.
[37] F. Touaiti, M. Pahlevan, R. Nilsson, P. Alam, M. Toivakka, M.P. Ansell, C.E. Wilen, Impact of functionalised dispersing agents on the mechanical and viscoelastic properties of pigment coating, Prog. Org. Coat. 76 (1) (2013) 101–106.
[38] Eric W.S. Hagan, Maria N. Charalambides, Christina R.T. Young, Thomas J. S. Learner, Stephen Hackney, Influence of the inorganic phase concentration and geometry on the viscoelastic properties of latex coatings through the glass-transition, Polymer 52 (7) (2011) 1662–1673.
[39] D.K. Makepeace, P. Locatelli, C. Lindsay, J.M. Adams, J.L. Keddie, Colloidal polymer composites: are nano-fillers always better for improving mechanical properties? J. Colloid Interface Sci. 523 (2018) 45–55.
[40] Warren Carl Oliver, George Mathews Pharr, An improved technique for determining hardness and elastic modulus using load and displacement sensing indentation experiments, J. Mater. Res. 7 (6) (1992) 1564–1583.
[41] Warren C. Oliver, Georges M. Pharr, Measurement of hardness and elastic modulus by instrumented indentation: advances in understanding and refinements to methodology, J. Mater. Res. 19 (1) (2004) 3–20.
[42] Tao Wang, Carolina de las Heras Alarcón, Monika Goikoetxea, Itxaso Beristain, Maria Paulis, Maria J. Barandiaran, José M. Asua, Joseph L. Keddie, Cross-linked network development in compatibilized alkyd/acrylic hybrid latex films for the creation of hard coatings, Langmuir 26 (17) (2010) 14323–14333.
[43] Manoli Zubitur, José M. Asua, Agitation effects in the semicontinuous emulsion polymerization of styrene and butyl acrylate, J. Appl. Polym. Sci. 80 (6) (2001) 841–851.
[44] J. Chen, S.J. Bull, On the factors affecting the critical indenter penetration for measurement of coating hardness, Vacuum 83 (6) (2009) 911–920.
[45] F. Deplace, C. Carelli, S. Mariot, H. Retsos, A. Chateauminois, K. Ouzineb, C. Creton, Fine tuning the adhesive properties of a soft nanostructured adhesive with rheological measurements, J. Adhes. 85 (1) (2009) 18–54.
[46] Robert S. Gurney, Damien Dupin, Juliana S. Nunes, Keltoum Ouzineb, Elodie Siband, José M. Asua, Steven P. Armes, Joseph L. Keddie, Switching off the tackiness of a nanocomposite adhesive in 30 s via infrared sintering, ACS Appl. Mater. Interfaces 4 (10) (2012) 5442–5452.
[47] Dirk Willem Van Krevelen, Klaas Te Nijenhuis, Properties of Polymers: Their Correlation With Chemical Structure; Their Numerical Estimation and Prediction From Additive Group Contributions, Elsevier, 2009.
[48] A. Eisenberg, T. Yokoyama, Emma Sambalido, Dehydration kinetics and glass transition of poly (acrylic acid), J. Polym. Sci., Part A-1: Polym. Chem. 7 (7) (1969) 1717–1728.

[49] Santanu Basu, U.S. Shivhare, A.S. Mujumdar, Moisture adsorption isotherms and glass transition temperature of xanthan gum, Dry. Technol. 25 (9) (2007) 1581–1586.
[50] Boris E. Gdalin, Eugenia V. Bermesheva, Georgy A. Shandryuk, Mikhail M. Feldstein, Effect of temperature on probe tack adhesion: extension of the dahlquist criterion of tack, J. Adhes. 87 (2) (2011) 111–138.
[51] Yang Liu, Agata M. Gajewicz, Victor Rodin, Willem-Jan Soer, Jurgen Scheerder, Guru Satgurunathan, Peter J. McDonald, Joseph L. Keddie, Explanations for water whitening in secondary dispersion and emulsion polymer films, J. Polym. Sci. B Polym. Phys. 54 (16) (2016) 1658–1674.
[52] Nicola Kessel, Derek R. Illsley, Joseph L. Keddie, The diacetone acrylamide crosslinking reaction and its influence on the film formation of an acrylic latex, J. Coat. Technol. Res. 5 (3) (2008) 285–297.
[53] Michael Rubinstein, Ralph H. Colby, in: Polymer Physics 23, Oxford university press, New York, 2003, p. 338, chapter 8.